Zheng, R., Cheng, Y., Jiang, X., Lin, T., Chen, W., Deng, G., Miras, H. N. and Song, Y.-F. (2022) Fiber templated epitaxially grown composite membranes: from thermal insulation to infrared stealth. *ACS Applied Materials and Interfaces*, 14(23), pp. 27214-27221. (doi: 10.1021/acsami.2c05906)

There may be differences between this version and the published version. You are advised to consult the published version if you wish to cite from it.

http://eprints.gla.ac.uk/273033/

Deposited on 13 June 2022

Enlighten – Research publications by members of the University of Glasgow
http://eprints.gla.ac.uk

# Fibre Templated Epitaxially Grown Composite Membranes: From Thermal Insulation to Infrared Stealth

Ruoxuan Zheng,[1] Yao Cheng,[1,2] Xiao Jiang,[1] Tong Lin,[1] Wei Chen,[1*] Gaofeng Deng,[3*] Haralampos N. Miras[4] and Yu-Fei Song[1*]

[1]State Key Laboratory of Chemical Resource Engineering, Beijing University of Chemical Technology, Beijing 100029, P. R. China. Tel/Fax: +86 10-64431832. *E-mail: chenw@mail.buct.edu.cn; songyf@mail.buct.edu.cn.

[2]Beijing Graphene Institute (BGI), Beijing, 100095, P. R. China.

[3]State Key Laboratory of Building Safety and Environment, China Academy of Building Research, Beijing, 100013, P. R. China. *E-mail: denggaofeng@cabrtech.com.

[4]WestCHEM, School of Chemistry, University of Glasgow, Glasgow, G12 8QQ, UK.

**ABSTRACT** Thermal insulation materials show a substantial impact on civil and military fields for applications. Fabrication of efficient, flexible, comfortable composite materials for thermal insulation is thereby of significance. Herein, a "Fibre Templated Epitaxial Growth" strategy was adopted to construct PAN@LDH (PAN = polyacrylonitrile; LDH = layered double hydroxides) composite membranes with a 3D network structure. The PAN@LDH showed an impressive temperature difference of 28.1 °C as thermal insulation material in the hot stage of 80 °C with a thin layer of 0.6 mm. Moreover, when a human hand was covered with 3-layers PAN@LDH-70%

composite membrane, it rendered invisible to infrared radiation. Such excellent performance can be attributed to the following reasons: 1) the hierarchical interfaces of PAN@LDH composite membrane reduced thermal conduction; 2) the 3D network structure of the PAN@LDH composite membranes restricted thermal convection; 3) the selective infrared absorption of LDHs decreased thermal radiation. When modified with Dodecyltrimethoxysilane (DTMS), the resulting PAN@LDH@DTMS membrane can be used under high humidity conditions with excellent thermal insulation properties. As such, this work provides a facile strategy for development of high-performance thermal insulation functional membranes.

**KEYWORDS:** Layered double hydroxides; PAN; Composite membrane; Thermal insulation; Infrared Stealth.

## INTRODUCTION

Thermal energy plays a vital role in industrial, construction, aerospace, batteries, thermal protective clothing, and other civil and military fields.[1-4] Efficient management of thermal energy could not only promote to reduce energy consumption and carbon dioxide emission, but also stabilize the operation of electronic equipment, and prolong the service life.[5-9] For example, by using thermal insultation materials properly, heat loss can be effectively diminished during generation, transportation, storage and utilization of thermal energy.[10-15] With rapid development of electronic devices and the improvement of military detection means in recent years, more and more strict requirements are put forward for thermal management, especially for thermal insulation and infrared stealth materials.[16-20] Among many thermal insulation materials, various nanofiber-based materials have been investigated widely due to the low density, specific heat capacity and thermal conductivity. For example, Zhang *et al.*[21] reported a wet-spinning approach for fabrication of Kevlar aerogel fibre, in which thermal insulation layers (KNA) and IR absorption surface layers (KNA/PCM) were developed to meet infrared stealth requirement; Cui *et al.*[22] demonstrated a dip-coated Ag nanowire-cloth with significantly high IR reflectance as well as thermal insulation capability over normal cloth, where the metallic nanowires formed a conductive network with excellent thermal insulation and reflected human body infrared radiation. Ding *et al.* [23] fabricated a superelastic lamellar-structured ceramic nanofibrous aerogels (CNFAs) with ultralow density, low thermal conductivity (0.025 W $m^{-1}$ $K^{-1}$) and fire resistance. Infrared stealth materials are highly demanded in military and

industrial application. [24]

Thermal infrared camera can detect the targets by comparing the difference of emission energy between the target and background. According to the Stefan-Boltzmann's law $W = \varepsilon\sigma T^4$ ($W$ = emission energy, $\varepsilon$ = infrared emissivity, $\sigma$ = constant of Stefan-Boltzmann, $T$ = absolute temperature), [25-26] when the temperature of target was higher than that of the background, the target can be easily detected by thermal infrared camera. When the target was covered by the thermal insulation material, the surface temperature was close to that of the background. As a result, the target was undetectable by thermal infrared camera. In another words, the material with excellent thermal insulation property can be a good candidate for thermal stealth material.[11]

As is well known, the heat transfer can be recognized as the sum of the thermal convection, thermal conduction and thermal radiation.[27]

$$\lambda = \lambda_{\mathrm{conv}} + \lambda_{\mathrm{cond}} + \lambda_{\mathrm{rad}}$$

Thermal convection ($\lambda_{\mathrm{conv}}$) is the phenomenon of heat release from a higher temperature to a lower temperature in the process of fluid flow. When the material is an airtight system or the inner hole size of material is less than 4 mm, the contribution of convection to heat transfer can be negligible.[28] Thermal conduction ($\lambda_{\mathrm{cond}}$) is a macroscopic expression of heat transfer from high temperature to low temperature caused by the thermal movement of molecules or atoms in the system and their interactions. There are two strategies to reduce thermal conduction. One is to reduce the solid component and reduce the continuous contact of materials; the other is to select materials with poor thermal conductivity. Thermal radiation is the phenomenon

that an object with a temperature higher than 0 K emits electromagnetic waves. The effective method to reduce thermal radiation is the improvement of the shielding ability against infrared radiation.

During the development of nanofiber-based thermal insulation materials, addition of inorganic materials has attracted wide interest. For example, Xie *et al.* [29] synthesized a novel hydroxyapatite nanowires/polyimide (HAnws/PI) composite aerogel with a 3D network structure, which resulted in high porosity (>96%) and low radial thermal conductivity (0.032W $m^{-1}$ $K^{-1}$). Yang *et al.* [30] proposed a 3D reticulated and hierarchically porous SiC/$Si_3N_4$ aerogels, exhibiting an ultrahigh porosity of 99.79% and low thermal conductivity of 0.023 W $m^{-1}$ $K^{-1}$. Wang *et al.* [31] fabricated a robust bio-based aerogel containing montmorillonite with 3D networks, which showed low thermal conductivity and high-temperature insulation.

Layered Double Hydroxides (LDHs) are a class of inorganic clay materials that consist of positively charged main laminate and interlaminar anions, and LDHs exhibit excellent selective infrared absorption ability and wide infrared absorption range.[32] Feng *et al.* [33] designed LDH/LDPE film with infrared absorption property, which exhibited enhanced heat retention effect. As such, LDHs are suitable to be utilized as infrared stealth material.[34]

In this work, we reported a “Fibre Templated Epitaxial Growth” strategy to construct a 3D network structure of PAN@LDH composite membrane materials. The *in-situ* growth of LDH into PAN was demonstrated to be able to reduce thermal conduction, restrict thermal convection and decrease thermal radiation. Excellent

thermal insulation of 28.1 °C with a thin layer of 0.6 mm was achieved. A human hand covered by 3-layers PAN@LDH-70% composite membrane realized invisible under infrared camera. More interestingly, when modified with DTMS, the resulting PAN@LDH@DTMS membrane showed an excellent thermal insulation under high humidity conditions.

## RESULTS AND DISCUSSION

As presented in Figure 1a-b, the hexagonal plates of LDHs with an average size of 2 μm were interpenetrated into PAN nanofiber, which was significantly different with the morphologies of PAN and PAN-AlOOH (Figure S1). Cross-section SEM image in Figure 1c exhibited that the LDH plate was "pierced" by PAN nanofibers. Furthermore, the embedded growth of LDH plates inside the PAN nanofiber was clearly displayed in HRTEM image in Figure 1d. A lattice fringe spacing of 0.23 nm corresponding to the (015) facet of LDH was shown in Figure 1e. Energy-dispersive X-ray measurement (EDX) elemental mapping (Figure 1f) showed that Mg, Al, C and O elements were uniformly dispersed on the surface of PAN@LDH composite membrane. Based on the morphologies of PAN membrane and PAN@LDH composite membrane, the corresponding roughness curves (Figure 1g-j) were obtained respectively.

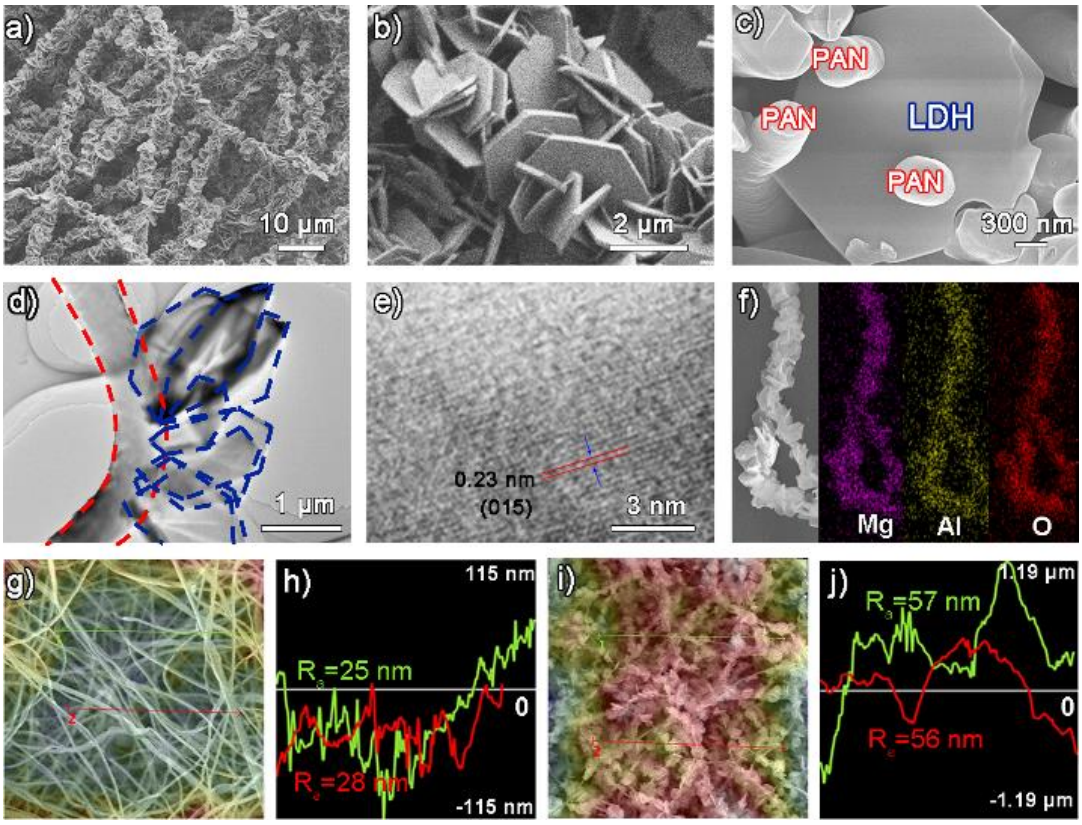


**Figure 1**. a-b) SEM images, c) Cross-section SEM image, d-e) HRTEM image, f) Elemental mapping images of Mg, Al and O of PAN@LDH composite membrane, respectively. Roughness curves of g-h) PAN membrane and i-j) PAN@LDH composite membrane in 3D roughness reconstruction system.

The roughness curves exhibited that the average roughness of PAN@LDH composite membrane was 56.5 nm, which was twice than that of PAN membrane (26.5 nm), indicating that the *in-situ* growth of LDH onto PAN dramatically improved the roughness. SEM images of PAN@LDH composite membrane with "Seeds Embedded" demonstrated the significance of the AlOOH for the *in-situ* growth of LDHs (Figure S2). When the PAN@LDH composite membrane was subjected to folding and rubbing, no LDH plates were peeled off, indicating the integrity and rigidity of the interpenetrated growth structure (Figure S3). XRD patterns of PAN@LDH membranes

showed the characteristic diffraction peaks of (003), (006), (012), (015) and (018) of LDH at 10.8°, 22.5°, 34.0°, 38.5°,46.0°, respectively (Figure S4a). FT-IR spectra of PAN@LDH membranes exhibited a peak at 1356 $cm^{-1}$, which resulted from the $CO_3^{2-}$ stretching vibration of LDH (Figure S4b). TGA and DTG curves of PAN@LDH membranes were shown in Figure S5. The weight loss ranging from 50 to 218 °C was attributed to the removal of water. The second weight loss in the range of 218-325 °C was due to the loss of interlaminar $CO_3^{2-}$. The third weight loss between 325 and 1000 °C was ascribed to carbonization and formation of mixed metal oxide.

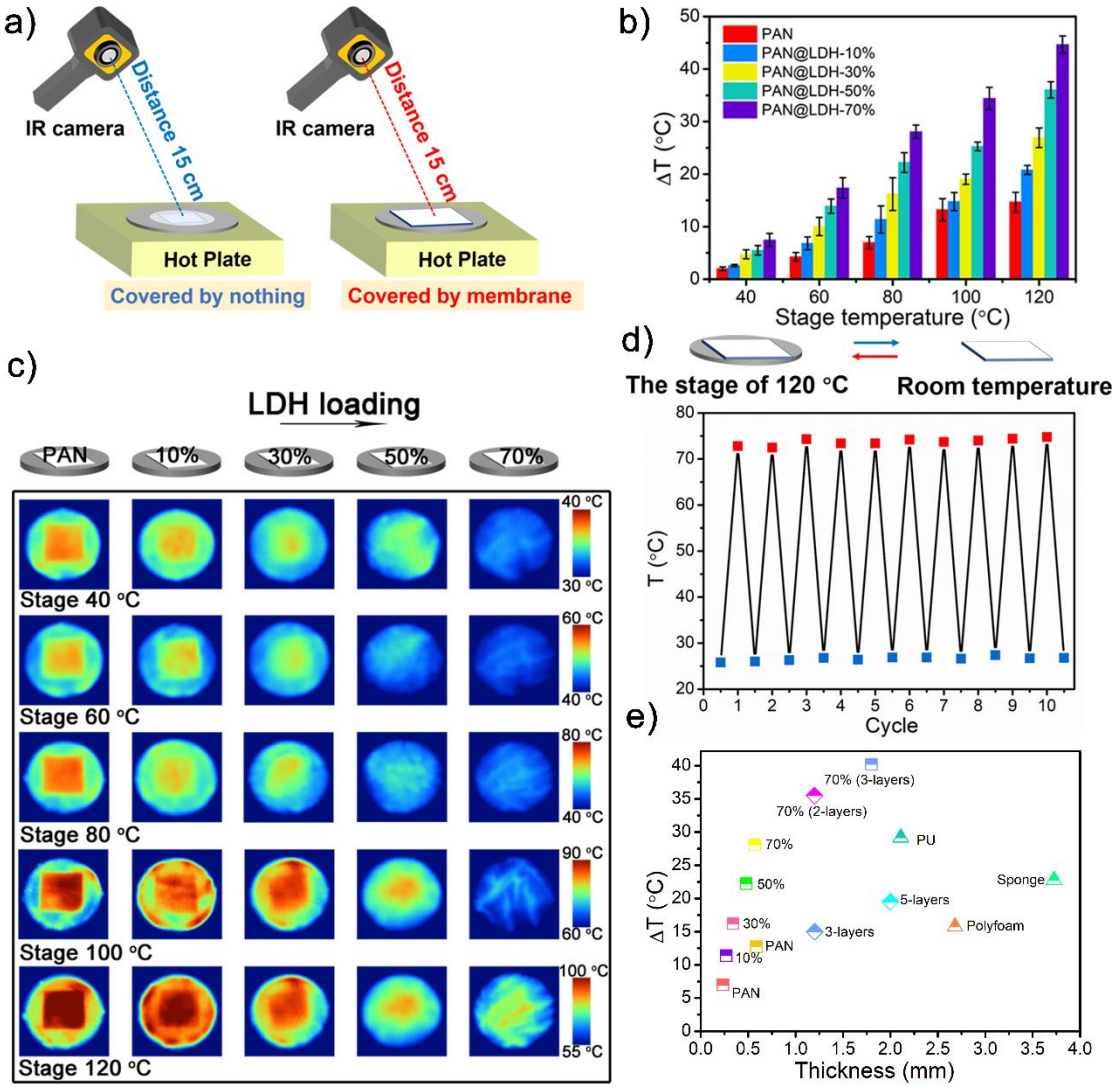


**Figure 2**. a) Test process diagram of thermal insulation. b) Temperature differences (ΔT) between

the hot plate and the surface of PAN membrane and PAN@LDH-x (x = 10, 30, 50 and 70%) composite membrane was plotted against the hot plate temperature, when the hot plate temperature was 40, 60, 80, 100 and 120 °C, respectively. c) Infrared images of PAN membrane and PAN@LDH-x (x = 10, 30, 50 and 70%) composite membrane when the stage temperature was 40, 60, 80, 100 and 120 °C, respectively. d) The temperature of the PAN@LDH-70% composite membrane surface when the stage was cyclically heated up and cooled down at a constant rate between 25 and 120 °C. e) Temperature difference (ΔT) between the stage (80 °C) and the surface of different thermal insulation materials corresponding the thickness of materials.

A melting point instrument equipped with temperature control was selected to provide the obtained stage temperature. The slide was placed in the center of the melting point instrument. The temperature of the slide square-shaped area was monitored using infrared camera (Figure 2a). As shown in Figure S6, the surface temperature of both PAN membrane and PAN@LDH-10% membrane rose greatly in the first 60 s, and PAN@LDH-10% membrane increased slightly slower than the PAN membrane. Finally, the surface temperature of PAN@LDH-10% membrane was lower than that of PAN membrane, indicating the *in-situ* growth of LDH led to an improved thermal insulation performance. The temperature differences (ΔT) of PAN membrane and PAN@LDH-x composite membranes were recorded to evaluate the thermal insulation performance when the hot stage temperature was 40, 60, 80, 100 and 120 °C, respectively, as shown in Figure 2b. Membranes with higher ΔT indicated better thermal insulation performance. There was a significant increase of ΔT when the LDH loading increased. Took the hot stage of 120 °C as an example, with the LDH loading increased from 0%

to 70%, the ΔT increased from 14.68 °C to 44.68 °C accordingly, showing an enhancement as high as 204.30%. The infrared images of PAN membrane and PAN@LDH-x composite membranes were compared when the hot stage temperature was 40, 60, 80, 100 and 120 °C, respectively (Figure 2c). The increased LDH loading ensured a dramatic decrease in the surface temperature, indicating the enhanced thermal insulation performance. To further test the dynamic thermal insulation property of the PAN@LDH composite membrane, the membrane was alternately placed at room temperature (25 ºC) and on the hot stage of 120 ºC every 2 min. The temperature variation was presented in Figure 2d. As the ambient temperature was cyclically changed between 25 ºC and 120 ºC, the PAN@LDH composite membrane surface also cycled between 25 and 75 ºC, a much narrower range. The measurement further indicated the potential of PAN@LDH composite membrane in thermal management by stabilizing thermal condition against environmental temperature change. When 2- and 3-layers of PAN@LDH composite membranes were applied to cover the hot stages, the surface temperature rose rapidly in the first 60 s. The more layers, the slower the temperature rose and the lower the final temperature was (Figure S7-S9). For the 3-layers PAN@LDH-70% composite membrane, ΔT was as high as 68.0 °C when the stage temperature was 120 °C. The thermal insulation effects of PAN, PAN@LDH-x composite membranes, PU, polyfoam and sponge were compared when the stage temperature was 80 °C (Figure 2e). The temperature difference of polyfoam and sponge were only 15.7 °C and 22.8 °C, with the thickness of 2.7 and 3.7 mm, respectively. It was surprising that the thermal insulation performance of PAN@LDH-70% composite

membrane was almost identical to PU, an excellent thermal insulation material, whereas the thickness of PAN@LDH-70% composite membrane was only 0.6 mm, less than 1/3 of the PU. The thermal insulation characteristics of PAN@LDH composite membrane and literature reports were listed in Table S1 for comparison. Based on the above comparison, the PAN@LDH composite membranes were demonstrated to be excellent thermal insulation materials. Even at the same thickness, the thermal insulation of PAN@LDH-70% composite membrane was 12.7 °C higher than PAN membrane (Figure S10). The thermal conductivity of PAN@LDH composite membrane was 0.036 W $m^{-1}$ $K^{-1}$. In addition, the density of PAN@LDH-70% composite membrane (69 $kg/m^3$) was lighter than other thermal insulation materials (Figure S11). The high flexibility and excellent processability of PAN@LDH composite membrane was also verified (Figure S12). The strain and stress of PAN@LDH composite membrane was 42.66% and 1.55 MPa, respectively. (Figure S13, Table S2).

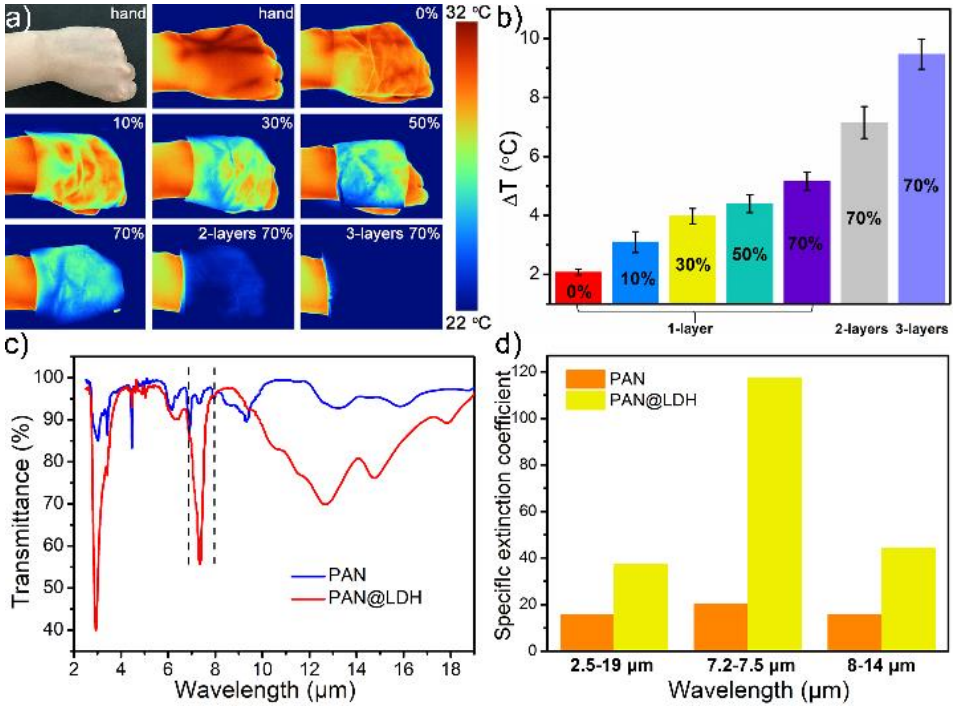


**Figure 3**. a) Infrared images of human skin covered by PAN membrane and PAN@LDH composite

membranes with different LDH loadings and layers. b) Temperature difference (ΔT) between the human hand and the surface of PAN membrane and PAN@LDH composite membrane with different LDH loadings and layers. c) ATR spectra of PAN membrane and PAN@LDH composite membrane. d) The specific extinction coefficients of PAN membrane and PAN@LDH composite membrane in 2.5-19 μm, 7.2-7.5 μm and 8-14 μm, respectively.

To confirm the potential of PAN@LDH composite membrane as thermal insulation material, we used a heating lamp in close to two identical candles with a length of 5 cm. One of the candles was covered with PAN@LDH composite membrane, while the other was not. For the former one, the candle covered with PAN@LDH composite membrane showed no signs of melting in 10 min, whereas for the latter one, the candle began to melt within 5 min and almost completely melted in 10 min (Figure S14).

We attempted to characterize the thermal insulation performance by covering PAN membrane and PAN@LDH-x composite membrane directly on the human skin. The infrared images and temperature differences were shown in Figure 3a-b. With the increasing LDH loading from 0% to 70%, the temperature difference increased from 2.08 °C to 5.17 °C. The 2-layers and 3-layers PAN@LDH-70% composite membrane showed better thermal insulation property. Apparently, the PAN@LDH-70% composite membrane displayed infrared shielding properties better than that of the PAN membrane. It's worth noting that when covered by 3-layers PAN@LDH-70% composite membrane, the human skin exhibited almost invisibility under the infrared camera. The infrared radiation contrast between the human skin covered by

PAN@LDH composite membrane and the background was too low to be detected by thermal infrared camera. In addition, the IR emissivity of PAN@LDH composite membrane was only 0.837 (Figure S15), while human skin was a good IR emitter with an IR emissivity as high as 0.98.[35] Low IR emissivity can decrease thermal radiation and as a result, the heat transfer decreases accordingly, which resulted in the improvement of thermal insulation. The infrared stealth characteristics of PAN@LDH composite membrane and the related reports were summarized in Table S3. As shown in Figure 3c, the ATR spectra of PAN membrane and PAN@LDH composite membrane showed a wide range of wavelength from 2.5 to 19 μm. The results demonstrated that the average infrared transmittance of PAN@LDH composite membrane was much lower than that of PAN membrane. Especially in the wavelength of 7.2-7.5 μm, the numerous $CO_3^{2-}$ presented in LDH led to a very low transmittance of 61.61%, while the transmittance of PAN membrane reached up to 94.5%. The transmittance had a great influence on the specific extinction coefficients (SEC). SEC showed the degree of radiation energy decay attributed to absorption and scattering, which reflected the ability to shield infrared radiation (see Table 1). Figure 3d showed that in the whole range of 2.5-19 μm, the SEC of PAN@LDH composite membrane was 37.18, while that of PAN membrane was only 15.73. It was surprising that the SEC of PAN@LDH composite membrane reached up to 117.5 in the range of 7.2-7.5 μm, which was an increase of more than 475% compared to the PAN membrane. It was well-known that human body emitted thermal radiation mainly in the mid-infrared range between 8 and 14 μm, in which the shielding of PAN@LDH composite membrane to infrared radiation

actually increased by 184.4% in comparison to PAN membrane.

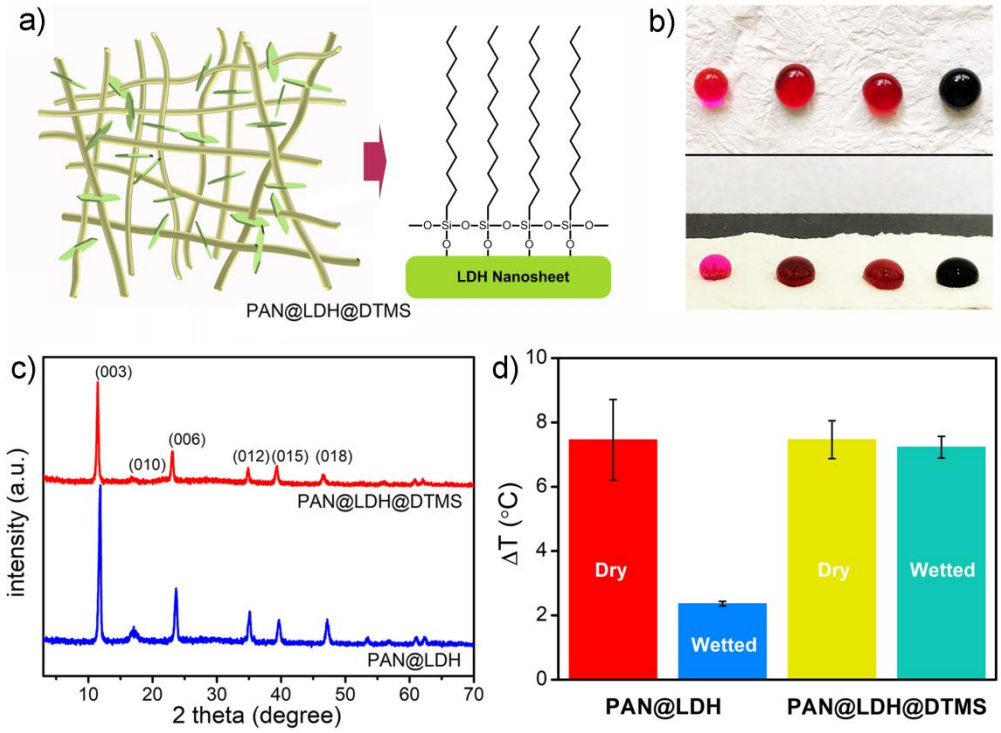


**Figure 4**. a) Schematic illustration of the modification with Dodecyltrimethoxysilane (DTMS). b) Surface wettability of PAN@LDH@DTMS composite membrane. c) XRD patterns of PAN@LDH and PAN@LDH@DTMS composite membranes, respectively. d) Thermal insulation performance of dry/wetted PAN@LDH composite membrane and PAN@LDH@DTMS composite membrane, respectively, when the hot plate temperature was 40 °C.

It is well established that the absorption of water within the pores of a material can decrease its thermal insulation performance dramatically [36-37] since the thermal conductivity of the water is 22.1 times that of air. Therefore, the hydrophobicity of thermal insulation material is an important property to be considered for practical application. [38-40] As shown in Figure 4a, abundant -OH in the LDH laminate can directly bond to Dodecyltrimethoxysilane (DTMS), rendering the LDH as an excellent candidate for hydrophobic modification. SEM image of PAN@LDH@DTMS

composite membrane showed that no obvious change in morphology when compared with PAN@LDH, in which LDH plate was still “pierced” by the PAN nanofiber (Figure S16). When the dyed water was dropped onto the surface of PAN@LDH@DTMS composite membrane, the water droplets stood steadily on the surface of membrane (Figure 4c), and the membrane supported the water droplet at a contact angle of 145° (Figure S17), confirming its hydrophobic nature. The XRD patterns of the PAN@LDH and PAN@LDH@DTMS composite membranes were shown in Figure 4c. As expected, the diffraction peaks of PAN@LDH@DTMS were assigned to the characteristic peak of LDH, indicating that the PAN@LDH@DTMS retained the crystal structure of LDH. When both PAN@LDH and PAN@LDH@DTMS composite membranes were wetted with water, the thermal insulation performances were compared as shown in Figure 4d. When the hot plate temperature was 40 ºC, the temperature difference of PAN@LDH membrane showed a sharp decline of 68%, while no significant decrease of thermal insulation performance was observed for PAN@LDH@DTMS membrane. Compared with PAN@LDH membrane, the PAN@LDH@DTMS composite membrane exhibited super-hydrophobicity and excellent thermal insulation under humid conditions and/or rainy weather. Both PAN@LDH and PAN@LDH@DTMS membranes can be used under different conditions such as cold protective clothing and pipeline protecting.

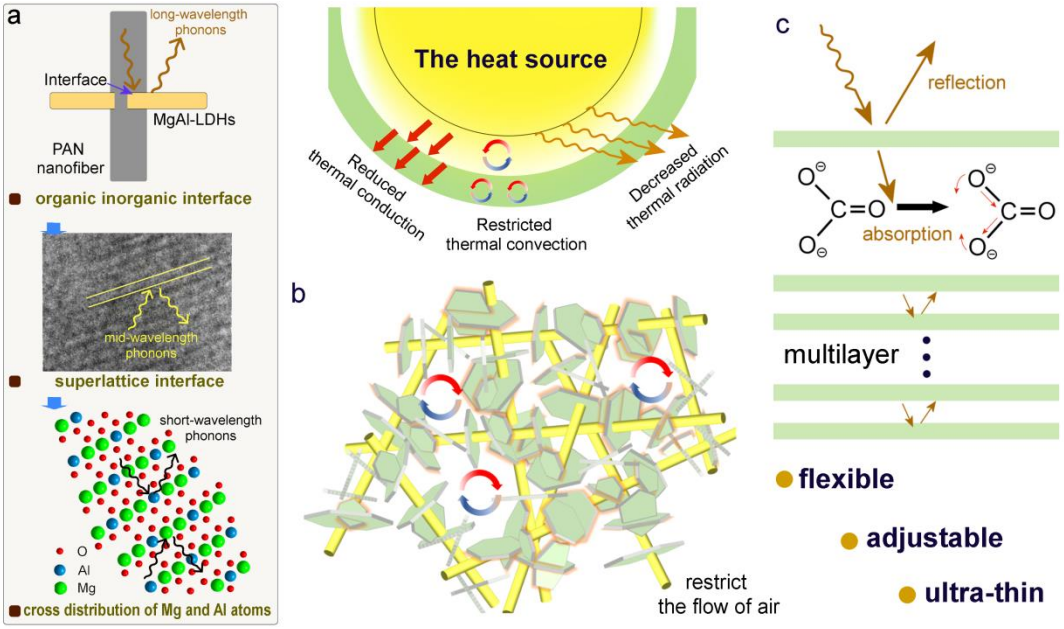


**Figure 5**. The proposed thermal insulation mechanism of a) Reduced thermal conduction, b) Restricted thermal convection and c) Decreased thermal radiation, respectively.

The thermal insulation mechanism was shown in Figure 5. Reduced thermal conduction played a vital role in thermal insulation. As shown in Figure 5a, the interfacial thermal resistance (ITR) with different length-scales reduced thermal conduction. Kapitza *et al.* [41] proved that the heat loss at the interface occurred when the heat transferred between different interface due to the presence of ITR. According to the quantum theory,[42] thermal conduction can be accomplished by energy transfer, and phonons are the carriers of energy. When materials contained the defects and interfaces, the phonons scattering can be increased and thereby the directional transmission of phonons decreased accordingly, resulting in the reduced thermal conduction. Compared with PAN, the improvement of surface roughness of PAN@LDH composite membrane greatly enhanced the diffuse reflection of phonons at the interface, and the phonons scattered at different angles, resulting in heat loss,

which is the main barrier limiting the efficient thermal conduction.[43] Phonons with different length-scales were more likely to be scattered by defects with comparable sizes.[42] Thus, for PAN@LDH composite membrane, the interface between LDH and PAN, the superlattice interface of LDH and the cross distribution of Mg and Al atoms strengthened long-wavelength, mid-wavelength and short-wavelength phonon scattering, respectively. The interpenetration of LDH confined air into pores, so that the thermal convection was restricted (Figure 5b). The thermal radiation emitted by the heat source was decreased due to the selective absorption of interlaminar $CO_3^{2-}$ and the multilayer reflection of LDH laminate (Figure 5c).

## CONCLUSIONS

In summary, a general and facile method for the synthesis of PAN@LDH composite membranes by the "Fibre Templated Epitaxial Growth" strategy was demonstrated. A series of PAN@LDH composite membranes with different LDH loadings were obtained. The *in-situ* templated growth of LDH into PAN nanofiber membrane gave rise to a 3D interpenetrated network structure, which exhibited excellent thermal insulation and infrared stealth performance. The temperature difference (ΔT) between hot stage (80 °C) and PAN@LDH-70% composite membrane was as high as 28.1 °C, using only a thin layer of 0.6 mm. Demonstration conducted on a human hand covered with 3-layers of PAN@LDH-70% composite membrane rendered it infrared invisible.

Such excellent thermal insulation and infrared stealth properties can be attributed

to the following reasons: 1) the hierarchical interfaces of the PAN@LDH composite membranes reduced thermal conduction; 2) the 3D network structure of the PAN@LDH composite membranes restricted thermal convection; 3) the outstanding infrared absorption of LDH decreased thermal radiation. When modified with DTMS, the resulting PAN@LDH@DTMS composite membrane revealed a contact angle of 145°, and the hydrophobic nature afforded its excellent thermal insulation property when used under high humidity conditions. This study provides a unique opportunity for the development of multifunctional thermal insulating and infrared stealth materials.

## EXPERIMENTAL SECTION

### Preparation of PAN@LDH composite membrane

PAN@LDH composite membranes were prepared as we previously reported.[44]

### Calculation of LDH load

$$\frac{m_1 - m_2}{m_1}$$

$m_1$ is the mass of PAN@LDH composite membrane after loading LDH, and $m_2$ is the mass of PAN-AlOOH membrane before loading LDH.

### Preparation of PAN@LDH@DTMS composite membrane:

0.4 mL of Dodecyltrimethoxysilane (DTMS) and PAN@LDH composite membrane (7.5^7.5 $cm^2$) were added to a single-mouth flask with 150 mL n-hexane as solvent, and the reaction mixture was reflux for 48 h under 80 °C. After finished the reaction, the obtained membrane was washed n-hexane (100 mL×2) and dichloromethane (100 mL× 2), respectively. The PAN@LDH@DTMS membrane was obtained after dried in an oven at 60 °C for 2 h.

**The calculation of specific extinction coefficients (SEC)**

$$e^* = -\frac{1}{\rho l} ln \frac{I}{I_0}$$

e* was the specific extinction coefficient, $\rho$ and $l$ is the density and thickness of the membrane, respectively. $I_0$ is the intensity of incident infrared light, $I$ is the intensity of transmitted infrared light.

**Table 1.** The density, thickness, the ratio of the intensity of incident infrared light to the intensity of transmitted infrared light of membranes.

| | $\rho$ | $l$ | $\frac{I}{I_0}$ | $\frac{I}{I_0}$ | $\frac{I}{I_0}$ |
|---|---|---|---|---|---|
| | ($g/cm^3$) | (cm) | (2.5-19 μm) | (7.2-7.5 μm) | (8-14 μm) |
| PAN | 0.1384 | 0.02 | 0.9574 | 0.9451 | 0.9577 |
| PAN@LDH | 0.0687 | 0.06 | 0.8579 | 0.6161 | 0.8328 |

**Materials Characterization:**

Fourier-transform infrared (FT-IR) spectra were performed on a Bruker Vector 22 infrared spectrometer. Polarizing microscope melting point tester was operated at 220~240 V. X-ray diffraction (XRD) patterns were carried out by using a Shimadzu XRD-6000 diffractometer with Cu Kα source. The morphologies were investigated by emission scanning electron microscope (Zeiss Supra 55) with an EDS detector and transmission electron microscope (Hitachi H-800). All infrared images were taken by a thermal imager (TiS750, Fluke Thermography). Infrared emissivity was measured by using a Dual-band emissivity measuring instrument (IR-2). The thermal conductivity was evaluated by the Hot Disk device (TPS 2500S, Hot Disk). The tensile strength of the membrane was tested by a CMT6104/ZWICK/Instron tensile tester with a loading

rate of 5 mm · $min^{-1}$. Nicolet 8700 FT-IR spectrometer was used to obtain ATR spectra. Contact angle was tested by a DSA100, Kruss contact angle meter.

## Supporting Information

SEM images, Optical images, XRD patterns, FTIR spectra, TGA and DTG curves, temperature variations curves, infrared images, temperature difference histogram, density, stress-strain curve, IR emissivity and contact angle.

## Acknowledgements

This research was supported by National Nature Science Foundation of China (22178019), the Opening Funds of State Key Laboratory of Building Safety and Built Environment and National Engineering Research Center of Building Technology, and the Fundamental Research Funds for the Central Universities (XK1802-6, XK1803-05, XK1902, 12060093063).

## References

(1) Papadopoulos, A. M. State of the Art in Thermal Insulation Materials and Aims for Future Developments. *Energy Build.* **2005**, *37*, 77-86.

(2) Shi, H. G.; Li, S. L.; Cheng, J. B.; Zhao, H. B.; Wang, Y. Z. Multifunctional Photothermal Conversion Nanocoatings Toward Highly Efficient and Safe High-Viscosity Oil Cleanup Absorption. *ACS Appl. Mater. Interfaces* **2021**, *13*, 11948-11957.

(3) Zhou, M.; Wang, J.; Zhao, Y.; Wang, G.; Gu, W.; Ji, G. Hierarchically Porous Wood-Derived

Carbon Scaffold Embedded Phase Change Materials for Integrated Thermal Energy Management, Electromagnetic Interference Shielding and Multifunctional Application. *Carbon* **2021**, *183*, 515-524.

(4) Wang, G.; Zhao, Y.; Yang, F.; Zhang, Y.; Zhou, M.; Ji, G. Multifunctional Integrated Transparent Film for Efficient Electromagnetic Protection. *Nanomicro Lett* **2022**, *14*, 65.

(5) Hu, F.; Wu, S.; Sun, Y. Hollow-Structured Materials for Thermal Insulation. *Adv. Mater.* **2019**, *31*, 1801001.

(6) Gu, W.; Sheng, J.; Huang, Q.; Wang, G.; Chen, J.; Ji, G. Environmentally Friendly and Multifunctional Shaddock Peel-Based Carbon Aerogel for Thermal-Insulation and Microwave Absorption. *Nanomicro Lett* **2021**, *13*, 102.

(7) Gu, W.; Wang, G.; Zhou, M.; Zhang, T.; Ji, G. Polyimide-Based Foams: Fabrication and Multifunctional Applications. *ACS Appl. Mater. Interfaces* **2020**, *12*, 48246-48258.

(8) Fernandez, J. E. Materials for Aesthetic, Energy-Efficient, and Self-Diagnostic Buildings. *Science* **2007**, *315*, 1807-1810.

(9) Ni, G.; Li, G.; Boriskina, S. V.; Li, H.; Yang, W.; Zhang, T.; Chen, G. Steam Generation under One Sun Enabled by a Floating Structure with Thermal Concentration. *Nat. Energy* **2016**, *1*, 16126.

(10) Yu, Z. L.; Yang, N.; Apostolopoulou-Kalkavoura, V.; Qin, B.; Ma, Z. Y.; Xing, W. Y.; Qiao, C.; Bergstrom, L.; Antonietti, M.; Yu, S. H. Fire-Retardant and Thermally Insulating Phenolic-Silica Aerogels. *Angew. Chem., Int. Ed.* **2018**, *130*, 4538-4542.

(11) Cui, Y.; Gong, H.; Wang, Y.; Li, D.; Bai, H. A Thermally Insulating Textile Inspired by Polar Bear Hair. *Adv. Mater.* **2018**, *30*, 1706807.

(12) Li, S. L.; Wang, J.; Zhao, H. B.; Cheng, J. B.; Zhang, A. N.; Wang, T.; Cao, M.; Fu, T.; Wang, Y. Z. Ultralight Biomass Aerogels with Multifunctionality and Superelasticity under Extreme Conditions. *ACS Appl. Mater. Interfaces* **2021**, *13*, 59231-59242.

(13) Shi, H. G.; Zhao, H. B.; Liu, B. W.; Wang, Y. Z. Multifunctional Flame-Retardant Melamine-Based Hybrid Foam for Infrared Stealth, Thermal Insulation, and Electromagnetic Interference Shielding. *ACS Appl. Mater. Interfaces* **2021**, *13*, 26505-26514.

(14) Randall, J. P.; Meador, M.; Jana, S. C. Tailoring Mechanical Properties of Aerogels for Aerospace Applications. *ACS Appl.Mater. Interfaces.* **2011**, *3*, 613-626.

(15) Si, Y.; Yu, J.; Tang, X.; Ge, J.; Ding, B. Ultralight Nanofibre-Assembled Cellular Aerogels with Superelasticity and Multifunctionality. *Nat. Commun.* **2014**, *5*, 5802.

(16) Han, T.; Bai, X.; Thong, J.; Li, B.; Qiu, C. W. Full Control and Manipulation of Heat Signatures: Cloaking, Camouflage and Thermal Metamaterials. *Adv. Mater.* **2014**, *26*, 1731-1734.

(17) Shen, L.; Zheng, B.; Liu, Z.; Wang, Z.; Lin, S. Dehdashti, S.; Li, E.; Chen, H. Large-Scale Far-Infrared Invisibility Cloak Hiding Object from Thermal Detection. *Adv. Opt. Mater.* **2015**, *3*, 1738-1742.

(18) Schittny, R.; Kadic, M.; Guenneau, S.; Wegener, M. Experiments on Transformation Thermodynamics: Molding the Flow of Heat. *Phys. Rev. Lett.* **2013**, *110*, 195901.

(19) Xu, H.; Shi, X.; Gao, F.; Sun, H.; Zhang, B. Ultrathin Three-Dimensional Thermal Cloak. *Phys. Rev. Lett.* **2014**, *112*, 54301.

(20) Gu, W.; Tan, J.; Chen, J.; Zhang, Z.; Zhao, Y.; Yu, J.; Ji, G. Multifunctional Bulk Hybrid Foam for Infrared Stealth, Thermal Insulation, and Microwave Absorption. *ACS Appl. Mater.*

*Interfaces* **2020**, *12*, 28727-28737.

(21) Liu, Z.; Lyu, J.; Fang, D.; Zhang, X. Nanofibrous Kevlar Aerogel Threads for Thermal Insulation in Harsh Environments. *ACS Nano* **2019**, *13*, 5703-5711.

(22) Hsu, P. C.; Liu, X.; Liu, C.; Xie, X.; Lee, H. R.; Welch, A. J.; Zhao, T.; Cui, Y. Personal Thermal Management by Metallic Nanowire-Coated Textile. *Nano Lett.* **2015**, *15*, 365-371.

(23) Si, Y.; Wang, X.; Dou, L.; Yu, J.; Ding, B. Ultralight and Fire-Resistant Ceramic Nanofibrous Aerogels with Temperature-Invariant Superelasticity. *Sci. Adv.* **2018**, *4*, 8925.

(24) Salihoglu, O.; Uzlu, H. B.; Yakar, O.; Aas, S.; Balci, O.; Kakenov, N.; Balci, S.; Olcum, S.; Suzer, S.; Kocabas, C. Graphene-Based Adaptive Thermal Camouflage. *Nano Lett.* **2018**, *18*, 4541-4548.

(25) Sheehan, D. P. Infrared Cloaking, Stealth, and the Second Law of Thermodynamics. *Entropy* **2012**, *14*, 1915-1938.

(26) Liu, X.-F.; Lai, Y.-K.; Huang, J.-Y.; Al-Deyab, S. S.; Zhang, K.-Q. Hierarchical $SiO_2$@$Bi_2O_3$ Core/Shell Electrospun Fibers for Infrared Stealth Camouflage. *J. Mater. Chem. C* **2015**, *3*, 345-351.

(27) Wicklein, B.; Kocjan, A.; Salazar-Alvarez, G.; Carosio, F.; Camino, G.; Antonietti, M.; Bergstrom, L. Thermally Insulating and Fire-Retardant Lightweight Anisotropic Foams Based on Nanocellulose and Graphene Oxide. *Nat. Nanotechnol.* **2015**, *10*, 277-283.

(28) Lee, O.-J.; Lee, K.-H.; Yim, T. J.; Kim, S. Y.; Yoo, K.-P. Determination of Mesopore Size of Aerogels from Thermal Conductivity Measurements. *J Non Cryst Solids* **2002**, *298*, 287-292.

(29) Zhu, J.; Zhao, F.; Peng, T.; Liu, H.; Xie, L.; Jiang, C. Highly Elastic and Robust Hydroxyapatite Nanowires/Polyimide Composite Aerogel with Anisotropic Structure for

Thermal Insulation. *Compos. B. Eng.* **2021**, *223*, 109081.

(30) Zhang, X.; Zhang, Y.; Qu, Y. N.; Wu, J. M.; Zhang, S.; Yang, J. Three-Dimensional Reticulated, Spongelike, Resilient Aerogels Assembled by SiC/$Si_3N_4$ Nanowires. *Nano Lett.* **2021**, *21*, 4167-4175.

(31) Ye, D.-D.; Wang, T.; Liao, W.; Wang, H.; Zhao, H.-B.; Wang, Y.-T.; Xu, S.; Wang, Y.-Z. Ultrahigh-Temperature Insulating and Fire-Resistant Aerogels from Cationic Amylopectin and Clay via a Facile Route. *ACS Sustainable Chem. Eng.* **2019**, *7*, 11582-11592.

(32) Zhu, H.; Tang, P.; Feng, Y.; Wang, L.; Li, D. Intercalation of IR Absorber into Layered Double Hydroxides: Preparation, Thermal Stability and Selective IR Absorption. *Mater. Res. Bull.* **2012**, *47*, 532-536.

(33) Wang, L.; Wang, L.; Feng, Y.; Feng, J.; Li, D. Highly Efficient and Selective Infrared Absorption Material Based on Layered Double Hydroxides for Use in Agricultural Plastic Film. *Appl Clay Sci* **2011**, *53*, 592-597.

(34) Guo, Y.; Wang, J.; Li, D.; Tang, P.; Leroux, F.; Feng, Y. Micrometer-Sized Dihydrogenphosphate-Intercalated Layered Double Hydroxides: Synthesis, Selective Infrared Absorption Properties, and Applications as Agricultural Films. *Dalton Trans.* **2018**, *47*, 3144-3154.

(35) Cai, L.; Song, A. Y.; Li, W.; Hsu, P. C.; Lin, D.; Catrysse, P. B.; Liu, Y.; Peng, Y.; Chen, J.; Wang, H.; Xu, J.; Yang, A.; Fan, S.; Cui, Y. Spectrally Selective Nanocomposite Textile for Outdoor Personal Cooling. *Adv. Mater.* **2018**, *30*, 1802152.

(36) Kulasinski, K.; Guyer, R.; Derome, D.; Carmeliet, J. Water Adsorption in Wood Microfibril-Hemicellulose System: Role of the Crystalline-Amorphous Interface.

*Biomacromolecules* **2015**, *16*, 2972-2978.

(37) Belbekhouche, S.; Bras, J.; Siqueira, G.; Chappey, C.; Lebrun, L.; Khelifi, B.; Marais, S.; Dufresne, A. Water Sorption Behavior and Gas Barrier Properties of Cellulose Whiskers and Microfibrils Films. *Carbohydr. Polym.* **2011**, *83*, 1740-1748.

(38) Lindström, S. B.; Karabulut, E.; Kulachenko, A.; Sehaqui, H.; Wågberg, L. Mechanosorptive Creep in Nanocellulose Materials. *Cellulose* **2012**, *19*, 809-819.

(39) Chen, M.; Coasne, B.; Guyer, R.; Derome, D.; Carmeliet, J. Role of Hydrogen Bonding in Hysteresis Observed in Sorption-Induced Swelling of Soft Nanoporous Polymers. *Nat. Commun.* **2018**, *9*, 3507.

(40) Mihranyan, A.; Llagostera, A. P.; Karmhag, R.; Stromme, M.; Ek, R. Moisture Sorption by Cellulose Powders of Varying Crystallinity. *Int. J. Pharm.* **2004**, *269*, 433-442.

(41) Kapitza, P. L. Heat Transfer and Superfluidity of Helium II. *Phys. Rev.* **1941**, *60*, 354-355.

(42) Li, Z.; Xiao, C.; Fan, S.; Deng, Y.; Zhang, W.; Ye, B.; Xie, Y. Dual Vacancies: An Effective Strategy Realizing Synergistic Optimization of Thermoelectric Property in BiCuSeO. *J. Am. Chem. Soc.* **2015**, *137*, 6587-6593.

(43) Giri, A.; King, S. W.; Lanford, W. A.; Mei, A. B.; Merrill, D.; Li, L.; Oviedo, R.; Richards, J.; Olson, D. H.; Braun, J. L.; Gaskins, J. T.; Deangelis, F.; Henry, A.; Hopkins, P. E. Interfacial Defect Vibrations Enhance Thermal Transport in Amorphous Multilayers with Ultrahigh Thermal Boundary Conductance. *Adv. Mater.* **2018**, *30*, 1804097.

(44) Cheng, Y.; Li, L.; He, W.; Chen, W.; Deng, G.; Song, Y.-F. Seeds Embedded Epitaxial Growth Strategy for PAN@LDH Membrane with Mortise-Tenon Structure as Efficient Adsorbent for Particulate Matter Capture. *Appl. Catal. B* **2020**, *263*, 118312.

## Table Of Contents

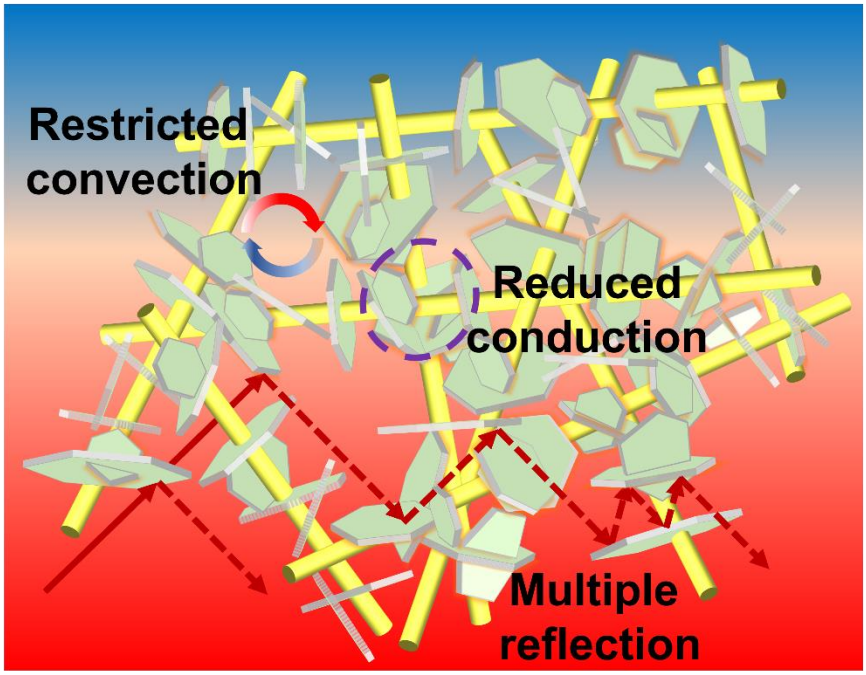


The *in-situ* templated growth of LDH into PAN nanofiber membrane gave rise to a 3D interpenetrated network structure, which exhibited excellent thermal insulation and infrared stealth performance.